

# Parallel Neural Local Lossless Compression

Mingtian Zhang<sup>1,2</sup>

James Townsend<sup>1</sup>

Ning Kang<sup>2</sup>

David Barber<sup>1</sup>

<sup>1</sup>AI Center, University College London,  
{m.zhang, james.townsend, d.barber}@cs.ucl.ac.uk  
<sup>2</sup>Huawei Noah’s Ark Lab  
kang.ning2@huawei.com

## Abstract

The recently proposed Neural Local Lossless Compression (NeLLoC) [27], which is based on a local autoregressive model, has achieved state-of-the-art (SOTA) out-of-distribution (OOD) generalization performance in the image compression task. In addition to the encouragement of OOD generalization, the local model also allows parallel inference in the decoding stage. In this paper, we propose two parallelization schemes for local autoregressive models. We discuss the practicalities of implementing the schemes and provide experimental evidence of significant gains in compression runtime compared to the previous, non-parallel implementation. The implementations of the proposed parallelized compression methods are available at <https://github.com/zmtomorrow/ParallelNeLLoC>.

## 1 Introduction

Lossless compression is an important application of probabilistic modelling. Given a model  $p_\theta(x)$  that approximates an underlying distribution  $p_d(x)$ , a lossless compressor can be built using  $p_\theta$ , with compression length approximately equal to  $-\log_2 p_\theta(x')$  for test data  $x'$ . Many models have been successfully used to compress image data, e.g. Variational Auto-Encoder (VAE) [11] based compressors [23, 24, 12, 18, 10] or flow based compressors [9, 1, 30], achieving significantly better compression rates than traditional codecs such as PNG [2] or WebP [13].

Most of the recent works on model-based compressors have focused on compressing test data  $x'$  that comes from the same distribution as the training data  $x' \sim p_d(x)$  [23, 12, 18, 9, 1, 30]. However, in practice, in downstream tasks data may come from a different distribution  $x' \sim p_o \neq p_d$ , and we would like to design probabilistic models with good out-of-distribution (OOD) generalization ability, whilst still achieving near state-of-the-art results on in-distribution test data.

Recent work [27] shows that it is possible for image models to generalize well to OOD data based on the following hypothesis [20, 8, 27, 29]: *local features (like smoothness, edges, corners etc.) are shared by different (natural) image distributions and dominate the log-likelihood, whereas non-local features (like semantics) are not shared*. Figure 1 gives a graphical illustration of the hypothesis. This hypothesis suggests that learning the non-local features that are specific to one distribution may hurt the OOD generalization performance, which has also been empirically verified in [27]. Therefore, to encourage OOD generalization, a local model can be used to build the lossless compressor. Under this intuition, paper [27] proposed the Neural Local Lossless Compressor (NeLLoC), which uses an autoregressive model with local dependency to ensure it can only learn local features.

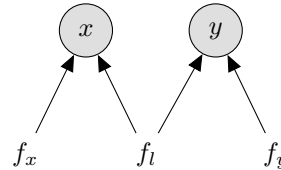


Figure 1: Graphical visualization of the hypothesis. We use  $x$  and  $y$  to represent two different image distributions  $p(x), p(y)$ ;  $f_l$  to indicate the shared local features and  $f_x, f_y$  are the non-local features that are specific to  $p(x)$  and  $p(y)$  respectively.

In addition to the OOD generalization encouragement, the local autoregressive models also have other fruitful properties for compression applications such as extremely small model size and the ability to compress images with arbitrary sizes, we refer readers to [27] for a detailed discussion. However, the decompression time of the original NeLLoC scales with  $O(D^2)$  for a  $D \times D$  image, which is a computation bottleneck for large images. In this paper, we propose a parallelization scheme that can improve the complexity from  $O(D^2)$  to  $O(D)$  on a machine without changing the compression rate. In the next section, we give a brief introduction to lossless compression with autoregressive models.

## 2 Lossless Compression with Autoregressive Models

Assuming each image  $\mathbf{x}$  has  $D \times D$  byte valued pixels  $x_{ij} \in \{0, \dots, 255\}$ . A *full autoregressive model* can be written as

$$p_f(\mathbf{x}) = \prod_{ij} p(x_{ij} | x_{[1:i-1, 1:D]}, x_{[i, 1:j-1]}), \quad (1)$$

where  $x_{[1:i-1, 1:D]} = \emptyset$  when  $i = 1$  and  $x_{[i, 1:j-1]} = \emptyset$  when  $j = 1$ . In practice, this full autoregressive model can be implemented by various structures, such as PixelRNN [25], PixelCNN [25, 19] or Transformers [4]. The model is then trained by minimizing the KL divergence between the data distribution  $p_d$  and the model  $p_f$ , which can be further approximated by a Monte-Carlo approximation with finite training data samples  $\{\mathbf{x}^1, \dots, \mathbf{x}^N\} \sim p_d(\mathbf{x})$

$$\text{KL}(p_d(\mathbf{x}) || p_f(\mathbf{x})) = - \int p_d(\mathbf{x}) \log p_f(\mathbf{x}) dx - H(p_d) \approx - \frac{1}{N} \sum_{n=1}^N \log p_f(\mathbf{x}^n) + \text{const.}, \quad (2)$$

where the entropy of the data distribution  $H(p_d)$  is a constant. Once we have learned the model  $p_f(\mathbf{x})$ , a stream coder is introduced to build a bijection between a given image  $\mathbf{x}'$  and a binary string  $s$  with length  $\text{len}(s) \approx -\log_2 p_f(\mathbf{x}')$ . When  $p_f \rightarrow p_d$ , the length  $-\log_2 p_f(\mathbf{x}')$  approaches the optimal compression length under Shannon’s source coding theorem [21]. Popular stream coders include Arithmetic Coding (AC) [26] and Asymmetric Numeral System (ANS) [6], we refer the reader to [14] and [22] for a detailed introduction of AC and ANS coders respectively.

Note that, for a full autoregressive model, the decoding of  $i$ th pixel of image  $\mathbf{x}'$  requires the distribution of  $x_i$ , which requires firstly decoding all the previous pixels  $x'_{1:i-1}$  to infer  $p(x_i | x'_1, \dots, x'_{i-1})$ . Therefore, the sequential inference mechanism in the decoding stage scales with  $O(D^2)$ .

### 2.1 Local Autoregressive Models

We define a *local autoregressive model*  $p_l(x)$  with *dependency horizon*  $h^1$ , to be an autoregressive model where each pixel depends only on previous pixels in a local region specified by  $h$ . To be precise, local model  $p_l(x)$  can be written as

$$p_l(\mathbf{x}) = \prod_{ij} p(x_{ij} | x_{[i-h:i-1, j-h:j+h]}, x_{[i, j-h:j-1]}), \quad (3)$$

with zero-padding used in cases where  $i$  or  $j$  are smaller than  $h$ . Figure 2b shows the dependency relationship between pixels in a local autoregressive model, compared to a full autoregressive model (Figure 2a), where each pixel depends on all previous pixels.

The local autoregressive model can be efficiently implemented by a simple modification of the PixelCNN structure [25, 27]. Specifically, given a dependency horizon  $h$ , the local PixelCNN can be constructed by letting the first masked convolutional layer have kernel height  $(h + 1)$  and width  $2h + 1$  and letting the subsequent layers be  $1 \times 1$  convolutions. In this case, the dependency horizon just depends on the kernel size of the first masked convolutional kernel.

The compression implementation provided in [27] uses a sequential inference mechanism that is the same as in the full autoregressive model, with time complexity in  $O(D^2)$ . However, for a local autoregressive model, there exist pixels that are conditional independent given the previous observed (decoded) pixels, allowing parallel inference in the decoding stage. In the following sections, we introduce an exact inference mechanism with runtime which scales with  $O(D)$  on a parallel machine and demonstrate a significant speedup experimentally.

<sup>1</sup>The dependency horizon  $h$  can also be interpreted as the *Chebyshev distance* [3] between pixels.

$x_{11}$	$x_{12}$	$x_{13}$	$x_{14}$	$x_{15}$
$x_{21}$	$x_{22}$	$x_{23}$	$x_{24}$	$x_{25}$
$x_{31}$	$x_{32}$	$x_{33}$	$x_{34}$	$x_{35}$
$x_{41}$	$x_{42}$	$x_{43}$	$x_{44}$	$x_{45}$
$x_{51}$	$x_{52}$	$x_{53}$	$x_{54}$	$x_{55}$

(a) Full autoregressive model

$x_{11}$	$x_{12}$	$x_{13}$	$x_{14}$	$x_{15}$
$x_{21}$	$x_{22}$	$x_{23}$	$x_{24}$	$x_{25}$
$x_{31}$	$x_{32}$	$x_{33}$	$x_{34}$	$x_{35}$
$x_{41}$	$x_{42}$	$x_{43}$	$x_{44}$	$x_{45}$
$x_{51}$	$x_{52}$	$x_{53}$	$x_{54}$	$x_{55}$

(b) Local autoregressive model with  $h = 1$ 

Figure 2: Comparison of full and local autoregressive models. In a full autoregressive model (a), the red pixel depends on all the previous pixels (in green), whereas in a local autoregressive model (b), the red pixel only depends on the previous pixels in a local region (in green).

### 3 Parallel Decoding with Local Autoregressive Models

In contrast to full autoregressive models, where pixels must be decoded sequentially, there exist pixels that can be independently decoded in a local autoregressive model. Figure 3 gives the topological order of parallel decoding, for a  $5 \times 5$  image, using a local autoregressive model with  $h = 1$ . The number in each pixel indicates the time at which the pixel can be decoded. For example, the two red pixels marked with time 6 can be decoded in parallel since they are independent under the model.

In general, for an image with size  $D \times D$ , on a machine with  $\lfloor \frac{D+h}{h+1} \rfloor$  parallel processing units, the total decoding time  $T = D + (D - 1) \times (h + 1)$ . Since  $h$  is a small constant  $h \ll D$ , the decoding time scales with  $\mathcal{O}(D)$ , which is a significant improvement over the  $\mathcal{O}(D^2)$  of full autoregressive models. In the example in Figure 3, for a  $5 \times 5$  image with dependency length  $h = 1$ , the decoding time is  $T = 13$  whereas in a full autoregressive model,  $T = 25$ . In the next section, we discuss how to implement the parallelization scheme in practice.

We observe that for fixed  $h$ , the positions of pixels decoded at each time step do not change. We can thus pre-compute the topological ordering and save the locations the pixels computed at each time step. At each time step in the decoding stage, we just load the saved positions of the independent pixels to be decoded and collect the image patches on which they depend into a batch. For example, for the pixel  $x_{33}$  in Figure 2b, the relevant patch is a  $3 \times 3$  square marked in red, the redundant pixels  $\{x_{33}, x_{34}, x_{42}, x_{43}, x_{44}\}$  will be masked out in the local autoregressive model. One can also take a rectangle patch that contains  $\{x_{22}, x_{23}, x_{24}, x_{32}, x_{33}, x_{34}\}$  to reduce the computation and  $\{x_{33}, x_{34}\}$  will be masked out in this case. We pad the patches with 0 for the pixels near the boundary, to make sure all the patches have the same size. The parallel decoding procedure is summarized in Algorithm 1.

1	2	3	4	5
3	4	5	6	7
5	6	7	8	9
7	8	9	10	11
9	10	11	12	13

Figure 3: Topological decoding order. Pixels with the same number are parallel decoded.

---

#### Algorithm 1 Parallel Decoding Procedure of Local Autoregressive Models

---

- 1: **for**  $t = 1$  to  $T$  **do**
  - 2:   Load the positions of independent pixels to be decoded at time  $t$ .
  - 3:   Gather the relevant patches based on the loaded positions to form a batch.
  - 4:   In parallel, compute the predictive distributions for those pixels using the batch.
  - 5:   Decode the pixel values using the predictive distributions.
  - 6: **end for**
- 

#### 3.1 Sheared Local Autoregressive Model

We notice that in Algorithm 1, the conditionally independent pixels in each step are located in nonadjacent positions in the images. For example, the dependent areas (green) of the two red pixels in Figure 3 are not aligned in memory. This requires extra indexing time when reading/writing their

---

**Algorithm 2** Parallel Decoding Procedure of Sheared Local Autoregressive Models
 

---

- 1: Shear the image based on the dependency horizon.
  - 2: **for**  $t = 1$  to  $T$  **do**
  - 3:     In parallel, compute the predictive distributions for those pixels in each column.
  - 4:     Decode the pixel values using the predictive distributions.
  - 5: **end for**
  - 6: Undo the shear operation for the decoded image.
- 

values. To alleviate the potential speed limitation, we propose to transform the model such that the conditionally independent pixels are aligned. Specifically, for a local autoregressive model with dependency horizon  $h$ , we shear the model, and image, with offset  $o = h + 1$ . Figure 4 shows an example where the local autoregressive model with  $h = 1$  (Figure 4a) is sheared with offset  $o = 2$ . We observe that in the sheared model, the conditionally independent pixels are aligned in memory, allowing significantly faster parallel reading/writing of those pixels. The sheared model has length  $L = D + (D - 1) \times o$  for a  $D \times D$  images, which is equal to the decoding steps  $T$  in pNeLLoC since  $o = h + 1$ . Therefore, the inference time also scales with  $O(D)$  on parallel processing units.

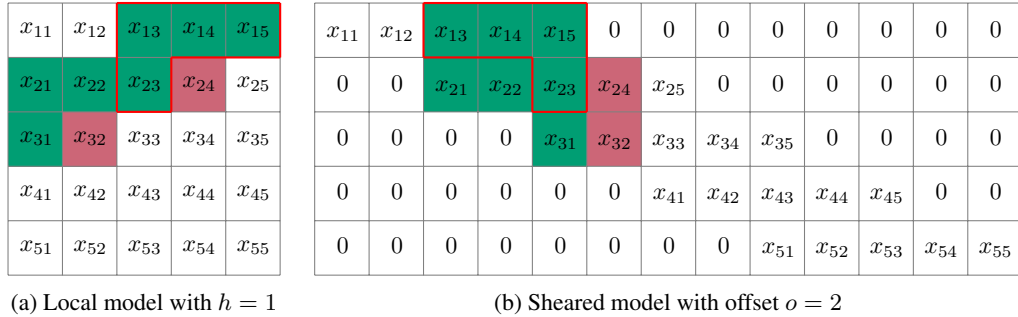


Figure 4: Pixel dependency after the shear operation. The red pixels in the same column in the sheared image (b) are conditionally independent given the green pixels, and are aligned in memory.

As discussed in Section 2, the pixel dependency structure of the local autoregressive model only depends on the first convolution kernel. Therefore, to shear the model, we only need to shear the first convolution kernel. Figure 5 visualizes the sheared convolutional kernel for two local autoregressive models with  $h = 1$  and  $h = 2$ . After shearing the model, we also need to shear the images to conduct compression and decompression, see Algorithm 2 for a summary of the decoding procedure. We refer to compression with the sheared model as **Sheared Local Lossless Compression (ShearLoC)**.

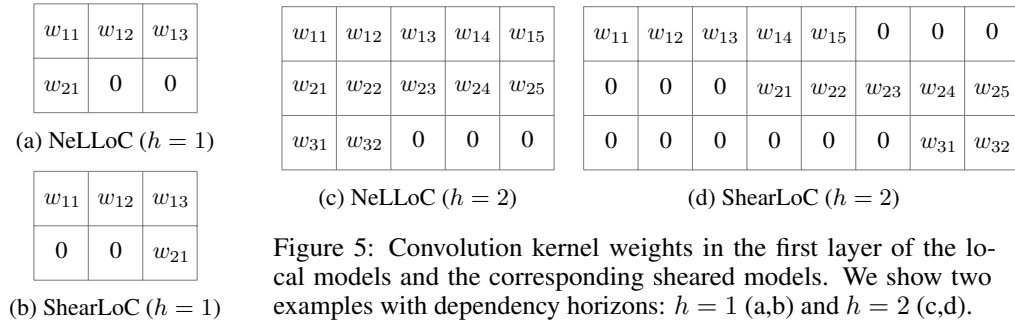


Figure 5: Convolution kernel weights in the first layer of the local models and the corresponding sheared models. We show two examples with dependency horizons:  $h = 1$  (a,b) and  $h = 2$  (c,d).

## 4 Demonstrations

We implement the compression model using PyTorch [15] with ANS. For the local autoregressive model, we use the same model architecture as that used in [27]: a local PixelCNN with horizon  $h = 3$ , followed by ResNet Blocks with  $1 \times 1$  convolution, see Appendix A.3 in [27] for details. We also use the three pre-trained (on CIFAR10) models (with 0, 1 and 3 ResNet blocks) provided by [27]

for all the experiments. The model with 3 ResNet blocks was shown by [27] to achieve SOTA OOD compression rate, see Table 6 of [27] for a detailed comparison with other compression methods. For reference, we report the model sizes and the test BPD on CIFAR10 for these three models in Table 1. During encoding, since all pixels are observed, the statistics of all the pixels can be computed in parallel. However, we have found that on CPU the computations may not be deterministic when using different batch sizes during the encoding and decoding. Therefore, we instead use the an identical inference procedure in both the encoding and decoding stages. Other details can be found in the provided repository. All the experiments are conducted on a MacBook Air (2020) with M1 chip and 8GB memory, the results are averaged over 10 images from the ImageNet [5] dataset.

Table 1: Test BPD on CIFAR10

Res. Num.	0	1	3
Size (MB)	0.49	1.34	2.75
BPD	3.38	3.28	3.25

We compare parallel NeLLOc (pNeLLOc) and ShearLoC with the original sequential NeLLOc (sNeLLOc) implementation. Since all algorithms use the same underlying pre-trained model, they have the same compression BPD. Table 2a shows the decompression time comparison using three models on images with side length 32. We find pNeLLOc is 2x faster than sNeLLOc with the 0 ResNet block model, and the improvement increases for larger models. Compared to pNeLLOc, ShearLoC achieves a further speed improvement, with a more significant advantage in larger models.

We also compare the decompression time on square images with increased side lengths: [32, 64, 128, 1024]<sup>2</sup>. Table 2b shows the improvement percentage from using pNeLLOc grows when we increase the size of the test images. This is consistent with the theoretical argument that the proposed parallelization scheme improves the computation complexity from  $O(D^2) \rightarrow O(D)$  on parallel units. Similarly, additional improvements can be achieved when using ShearLoC, which shares the same complexity with pNeLLOc but has more efficient memory access.

Table 2: Decoding time (s) comparisons. We show the improvement of pNeLLOc (in green) and ShearLoC (in red) comparing to using sNeLLOc.

(a) Different model sizes, the image has size  $32 \times 32$ .

Res. Num.	0	1	3
BPD	3.39	3.32	3.29
sNeLLOc	0.460 (-)	0.578 (-)	0.774 (-)
pNeLLOc	0.223 (2.06x)	0.277 (2.09x)	0.335 (2.31x)
ShearLoC	0.218 (2.11x)	0.222 (2.60x)	0.245 (3.16x)

(b) Different image sizes, the model has 0 ResNet blocks.

Side len.	32	64	128	1024
BPD	3.39	3.05	2.93	2.22
sNeLLOc	0.460 (-)	1.879 (-)	7.574 (-)	475.9 (-)
pNeLLOc	0.223 (2.06x)	0.757 (2.48x)	2.217 (3.42x)	100.0 (4.58x)
ShearLoC	0.218 (2.11x)	0.612 (3.07x)	1.683 (4.60x)	73.00 (6.52x)

## 5 Discussion

Several methods have been proposed to improve the sampling runtime in autoregressive models. For example, [17, 16] explore the multi-scale structure in the image domain, and design models that allow parallel generation of pixels in higher resolution samples conditioned on low resolution samples. In contrast to previous works, the parallel method proposed in this paper is specially designed for local autoregressive models, with the flexibility to handle images of arbitrary size. Local autoregressive models can also be combined with latent variable models to generate semantically-coherent images [7, 28]. In this case, the proposed parallelization schemes can be also used to improve the sampling efficiency, which we leave to future work.

<sup>2</sup>The  $1024 \times 1024$  images are provided in the repository, the corresponding result is averaged over 3 images.

## References

- [1] R. v. d. Berg, A. A. Gritsenko, M. Dehghani, C. K. Sønderby, and T. Salimans. Idf++: Analyzing and improving integer discrete flows for lossless compression. *International Conference on Learning Representations*, 2021.
- [2] T. Boutell and T. Lane. Png (portable network graphics) specification version 1.0. *Network Working Group*, pages 1–102, 1997.
- [3] C. D. Cantrell. *Modern mathematical methods for physicists and engineers*. Cambridge University Press, 2000.
- [4] R. Child, S. Gray, A. Radford, and I. Sutskever. Generating long sequences with sparse transformers. *arXiv preprint arXiv:1904.10509*, 2019.
- [5] J. Deng, W. Dong, R. Socher, L.-J. Li, K. Li, and L. Fei-Fei. Imagenet: A large-scale hierarchical image database. In *2009 IEEE conference on computer vision and pattern recognition*, pages 248–255. Ieee, 2009.
- [6] J. Duda. Asymmetric numeral systems: entropy coding combining speed of huffman coding with compression rate of arithmetic coding. *arXiv preprint arXiv:1311.2540*, 2013.
- [7] I. Gulrajani, K. Kumar, F. Ahmed, A. A. Taiga, F. Visin, D. Vazquez, and A. Courville. Pixelvae: A latent variable model for natural images. *International Conference on Learning Representations*, 2017.
- [8] J. D. D. Havtorn, J. Frellsen, S. Hauberg, and L. Maaløe. Hierarchical vaes know what they don’t know. In *International Conference on Machine Learning*, pages 4117–4128. PMLR, 2021.
- [9] E. Hoogeboom, J. W. Peters, R. v. d. Berg, and M. Welling. Integer discrete flows and lossless compression. *Neural Information Processing Systems*, 2019.
- [10] D. Kingma, T. Salimans, B. Poole, and J. Ho. Variational diffusion models. *Advances in neural information processing systems*, 34:21696–21707, 2021.
- [11] D. P. Kingma and M. Welling. Auto-encoding variational bayes. *International Conference on Learning Representations*, 2014.
- [12] F. Kingma, P. Abbeel, and J. Ho. Bit-swap: Recursive bits-back coding for lossless compression with hierarchical latent variables. In *International Conference on Machine Learning*, pages 3408–3417. PMLR, 2019.
- [13] L. Lian and W. Shilei. Webp: A new image compression format based on vp8 encoding. *Microcontrollers & Embedded Systems*, 3, 2012.
- [14] D. J. MacKay. *Information theory, inference and learning algorithms*. Cambridge university press, 2003.
- [15] A. Paszke, S. Gross, F. Massa, A. Lerer, J. Bradbury, G. Chanan, T. Killeen, Z. Lin, N. Gimelshein, L. Antiga, A. Desmaison, A. Kopf, E. Yang, Z. DeVito, M. Raison, A. Tejani, S. Chilamkurthy, B. Steiner, L. Fang, J. Bai, and S. Chintala. Pytorch: An imperative style, high-performance deep learning library. In H. Wallach, H. Larochelle, A. Beygelzimer, F. d’Alché-Buc, E. Fox, and R. Garnett, editors, *Advances in Neural Information Processing Systems 32*, pages 8024–8035. Curran Associates, Inc., 2019. URL <http://papers.neurips.cc/paper/9015-pytorch-an-imperative-style-high-performance-deep-learning-library.pdf>.
- [16] A. Razavi, A. van den Oord, and O. Vinyals. Generating diverse high-fidelity images with vq-vae-2. In *Advances in neural information processing systems*, pages 14866–14876, 2019.
- [17] S. Reed, A. Oord, N. Kalchbrenner, S. G. Colmenarejo, Z. Wang, Y. Chen, D. Belov, and N. Freitas. Parallel multiscale autoregressive density estimation. In *International Conference on Machine Learning*. PMLR, 2017.

- [18] Y. Ruan, K. Ullrich, D. Severo, J. Townsend, A. Khisti, A. Doucet, A. Makhzani, and C. J. Maddison. Improving lossless compression rates via monte carlo bits-back coding. In *International Conference on Machine Learning*. PMLR, 2021.
- [19] T. Salimans, A. Karpathy, X. Chen, and D. P. Kingma. Pixelcnn++: Improving the pixelcnn with discretized logistic mixture likelihood and other modifications. *arXiv preprint arXiv:1701.05517*, 2017.
- [20] R. T. Schirrmeister, Y. Zhou, T. Ball, and D. Zhang. Understanding anomaly detection with deep invertible networks through hierarchies of distributions and features. In *Neural Information Processing Systems*, 2020.
- [21] C. E. Shannon. A mathematical theory of communication. *ACM SIGMOBILE mobile computing and communications review*, 5(1):3–55, 2001.
- [22] J. Townsend. A tutorial on the range variant of asymmetric numeral systems. *arXiv preprint arXiv:2001.09186*, 2020.
- [23] J. Townsend, T. Bird, and D. Barber. Practical lossless compression with latent variables using bits back coding. *International Conference on Learning Representations*, 2019.
- [24] J. Townsend, T. Bird, J. Kunze, and D. Barber. Hilloc: Lossless image compression with hierarchical latent variable models. *International Conference on Learning Representations*, 2020.
- [25] A. Van Oord, N. Kalchbrenner, and K. Kavukcuoglu. Pixel recurrent neural networks. In *International Conference on Machine Learning*, pages 1747–1756. PMLR, 2016.
- [26] I. H. Witten, R. M. Neal, and J. G. Cleary. Arithmetic coding for data compression. *Communications of the ACM*, 30(6):520–540, 1987.
- [27] M. Zhang, A. Zhang, and S. McDonagh. On the out-of-distribution generalization of probabilistic image modelling. In *Neural Information Processing Systems*, 2021.
- [28] M. Zhang, T. Z. Xiao, B. Paige, and D. Barber. Improving vae-based representation learning. *arXiv preprint arXiv:2205.14539*, 2022.
- [29] M. Zhang, A. Zhang, T. Z. Xiao, Y. Sun, and S. McDonagh. Out-of-distribution detection with class ratio estimation. *arXiv preprint arXiv:2206.03955*, 2022.
- [30] S. Zhang, N. Kang, T. Ryder, and Z. Li. iflow: Numerically invertible flows for efficient lossless compression via a uniform coder. In *Neural Information Processing Systems*, 2021.